CPW-Fed Slotted Hexagonal-Shaped Antenna with Circular Splits for Ultra Wideband Applications

D. Aissaoui[1], A. Chaabane[2],A. Bouacha[3], and A. T. Denidni[4]

[1]Telecommunications and Smart Systems Laboratory, University of Djelfa, PO Box 3117, Djelfa 17000, Algeria
[2]Faculty of Technology, Department of Electronics, University of Ferhat Abbas Setif-1, Setif 19000, Algeria.
[3]Laboratoire de Télécommunications, Université de Tlemcen, BP 230, Pôle Chetouane, 13000, Tlemcen, Alegria
[4]Institute National De La Recherche Scientifique, INRS, 800, Rue De La Guichetière Ouest, Montréal, H5A1K6, Quebec, Canada

Corresponding author: D. Aissaoui (e-mail: djelloul.aissaoui@univ-djelfa.dz)

ABSTRACT This paper presents a coplanar waveguide-fed (CPW) slotted hexagonal-shaped antenna for ultra-wideband (UWB) applications. The proposed antenna consists of a radiating patch with a standard hexagonal shape. Fractal structures are etched into the hexagonal radiating patch to increase the impedance bandwidth. These fractal structures are formed by etching five different slots into the radiating element. The antenna is designed at 3 GHz on an RO4350B substrate, with a compact footprint of $0.388\ \lambda_0 \times 0.364\ \lambda_0 \times 0.015\ \lambda_0$ at 2.98 GHz. A prototype was fabricated and tested to validate the simulation results. Measurements performed with a well-calibrated Agilent 8722ES vector network analyzer show that the proposed antenna achieves a -10 dB bandwidth covering 2.98 GHz to 11.8 GHz, corresponding to 119.35%. Radiation patterns measured in an anechoic chamber exhibit stable and well-defined characteristics across the band. Furthermore, the antenna demonstrates high efficiency and reasonable realized gain over the entire operating bandwidth. Hence, the proposed antenna is a suitable candidate for many modern UWB wireless systems.

INDEX TERMS Fractal Antenna, Ultra Wideband Antenna (UWB), Coplanar Waveguide Fed (CPW), Hexagonal-shaped, Slot.

I. INTRODUCTION

ULTRA-Wideband (UWB) technology has emerged as one of the most rapidly advancing fields in wireless communications, driven by its inherent advantages of high data rates, low power spectral density, and robustness to interference across large frequency bandwidths. Concur-rently, modern telecommunication systems impose stringent requirements such as compact size, stable radiation patterns, and consistent gain over wide operating bands. These chal-lenges have motivated extensive research toward innovative antenna designs capable of meeting these demands [1], [2].

Among the various approaches, fractal geometries have proven to be a promising solution due to their unique properties of self similarity and space filling c apability. Their integration into conventional antenna structures enables key advantages such as miniaturization, bandwidth enhancement, and multiband operation [3]. Techniques such as slotting near the radiating edges have also been widely used to improve impedance bandwidth, as exemplified by the steering shaped design composed of a circular ring with elliptical spokes [4]. A wide variety of fractal antenna geometries have been inves-tigated for UWB applications, as reported in [5]–[16]. These designs target different performance objectives, including size reduction [5], [10], bandwidth enhancement through resonance control [13], [14], and multiband functionality [8], [9]. For example, hybrid Sierpinski–Koch fractal geometries have been employed to achieve compact radiators with pattern diversity [6], while bio inspired fractal shapes such as cauliflower like [5], floral like [7], and flower shaped [9] structures have been proposed to flexibly tune reso-nant frequencies. Other designs incorporate defected ground structures [9] or hybrid fractal patterns inspired by Giuseppe Peano and Sierpinski carpets [16] to further enhance perfor-mance.

However, many of these designs exhibit limitations in terms of UWB coverage or physical size. In [13], a combination of Koch curve and self affine fractal geometries achieves a wideband response from 1.6 to 3.4 GHz, but this does not cover the full UWB range (3.1–10.6 GHz) and the antenna dimensions are relatively large (66×27 mm^2). In [14], a staircase fractal curve applied to a truncated corner square patch antenna enables super wideband operation from 0.1 to 30 GHz, yet the bandwidth enhancement comes at the cost of a large footprint (60×60 mm^2). Similarly, [10] introduces a pentagon slot inside a fractal circular patch over a partial ground plane using a third iteration fractal geometry,

but the resulting wideband (4.5–9.3 GHz) covers only part of the UWB spectrum, missing both the lower and upper portions. In [6], a compact two element UWB MIMO antenna using a hybrid Sierpinski–Koch fractal radiator covers the UWB band except the WLAN band, and pattern diversity is achieved via a stub for isolation. Among the cited works, [5] demonstrates a cauliflower shaped fractal along the radiator edges, achieving an impedance bandwidth of 113% (3.05–10.96 GHz), a peak gain of about 6 dBi, and an average radiation efficiency above 90% across the band, representing one of the more complete UWB coverages.

Despite these recent advancements, several challenges remain. Many fractal UWB antennas still suffer from critical trade offs between size, bandwidth, and structural complexity. Some designs achieve wide bandwidth at the expense of increased physical dimensions, while others remain compact but fail to fully cover the standard UWB frequency range. Additionally, certain approaches introduce complex geometries or require elaborate ground plane modifications, making fabrication and integration more challenging. The problem statement of this paper is that these trade offs prevent existing designs from simultaneously achieving compactness, full band coverage, and stable performance. The design goals are therefore to develop a compact CPW fed slotted hexagonal antenna that: (1) covers the full UWB spectrum, (2) maintains good impedance matching (S11 $<$ -10 dB) over the entire band, (3) provides stable radiation patterns and acceptable gain, (4) ensures high radiation efficiency ($>$90%), and (5) keeps a reduced electrical footprint suitable for integra-tion into modern wireless systems. The design constraints that must be satisfied are: a compact electrical size, 50 Ω impedance matching across a very wide frequency range, use of a low loss substrate for high efficiency, manufacturability without overly complex or multilayer structures, and preser-vation of radiation stability across the entire UWB band. Satisfying all these constraints simultaneously constitutes the core challenge and the main contribution of this work.

This paper proposes a compact, CPW fed slotted hexagonal antenna with an embedded fractal geometry. The design aims to cover the full UWB spectrum, maintain good impedance matching, provide stable radiation patterns and acceptable gain, and ensure high radiation efficiency, all while keeping a reduced electrical footprint. Achieved results indicate that the antenna achieves wideband coverage (2.98–11.8 GHz, 119.35% fractional bandwidth), stable radiation characteristics, and high efficiency (peak 95.78% at 10 GHz), positioning it as a strong candidate for modern UWB applications such as IoT, wearable devices, and high speed wireless communication systems.

II. ANTENNA DESCRIPTION AND RESULTS

Figure 1 depicts the physical layout of the proposed slotted hexagonal antenna, featuring a hexagonal radiating patch embedded with five strategically etched slots of varying geometries. To ensure self-similarity and a consistent fractal behavior, these slots are designed based on a recursive scaling process. Mathematically, the dimensions of the nth iteration are governed by the following recursive system:

$$R_n = A_n \cdot (0.866 \cdot t) \tag{1}$$

$$A_{n+1} = \frac{R_n}{t_1} \tag{2}$$

where:

- $A_0 = 11.5$ mm is the initial side length of the hexagonal patch,
- R_n is the radius of the circular slot at the nth iteration,
- A_n is the side length of the hexagonal structure at the nth iteration,
- $t = 0.8$ and $t_1 = 0.985$ are the scaling factors used to optimize the impedance bandwidth.

By applying these equations for $n = 0, 1, 2, 3, 4$, the precise dimensions of the five etched slots are obtained, maintaining the fractal nature of the radiating element.

These slots are meticulously positioned to modify the surface current distribution, thereby enhancing impedance bandwidth through multi-resonance excitation. Figure 2 outlines the iterative design evolution, highlighting how successive modifications—such a s s lot i ntegration a nd g round plane optimization—improve the antenna's performance metrics. Notably, the removal of material from the radiator's central region, where current density is inherently low, enables weight reduction and contributes to miniaturization without compromising radiation efficiency. T his a pproach n ot only reduces conductor losses but also improves design adaptability for integration into space-constrained devices.

Further enhancements include the truncation of the ground plane's outer corners, a critical modification t hat minimizes impedance mismatch and extends bandwidth by suppressing unwanted surface-wave propagation. The antenna is fabricated on an RO4350B substrate ($\varepsilon_r = 3.48$, $\tan\delta = 0.0037$), chosen for its low-loss properties and thermal stability. Its compact electrical dimensions are $0.391\lambda_0 \times 0.366\lambda_0 \times 0.015\lambda_0$ at 3 GHz. While the hexagonal patch approaches the electromagnetic behavior of a circular radiator, its angular geometry simplifies fabrication precision a nd introduces sharper edges that can support edge diffraction for broader bandwidth.

The fundamental resonant frequency (f_r) of the hexagonal monopole is derived using Equation (1), adapted from the equivalent circular monopole theory described in [17], which accounts for substrate permittivity and patch geometry. Equation (2) calculates the hexagonal perimeter, enabling an accurate estimation of the relationship between physical dimensions and operational bandwidth. These equations underpin the design's scalability, allowing frequency tuning for diverse UWB applications, from medical imaging and radar systems to high-speed data links.

$$f_r = \frac{J_{mn}\, c}{2\pi r \sqrt{1 + \frac{2t}{\pi r \varepsilon_r}\left(\ln\frac{\pi r}{2t} + 1.7726\right)}} \tag{3}$$

$$f_r = \frac{r}{3^{3/4}}\sqrt{2\pi\left[1+\frac{2t}{\pi r\varepsilon_r}\left(\ln\frac{\pi r}{2t}+1.7726\right)\right]} \quad (4)$$

Here, ε_r is the dielectric constant of the substrate; c is the speed of light in free space; t is the height (thickness) of the dielectric substrate; r corresponds to the effective radius of the equivalent circular radiating patch; and J_{mn} is the mth zero of the Bessel function of order n. Selected values of J_{mn} are provided in Table 1.

TABLE 1. Paramèters of roots with variation in modes

Mode (n, m)	J_{mn}
0.1	0
1.1	1.84118
2.1	3.05424
0.2	3.83171
3.1	4.20119

Deriving an accurate lumped-element equivalent circuit for the proposed fractal antenna is challenging due to its complex geometry and strongly distributed electromagnetic interactions; any simplified representation would likely be either overly approximate or excessively complex. Therefore, the design methodology primarily relies on full-wave electromagnetic simulations, supported by surface current distribution analysis. To provide a theoretical design framework, recursive scaling formulas (Eqs. (1)–(2)) are introduced to define the fractal slot dimensions, along with resonant frequency formulations (Eqs. (3)–(4)).

To achieve good performance, the dimensions of the proposed slotted hexagonal antenna were optimized. The final physical parameters are listed in Table 2.

TABLE 2. Physical Dimensions of the proposed antenna.

Parameter	Value [mm]	Parameter	Value [mm]
L_{g1}	8.89	L_{h2}	13.97
L_{g2}	3.048	w_{h2}	16.002
w_{f1}	3.556	L_{h3}	9.906
w_{f2}	2.54	w_{h3}	11.176
w_{g1}	17.526	L_{h4}	6.858
w_{g2}	13.462	w_{h4}	7.874
w_{g3}	3.556	L_{h5}	4.826
d	3.81	w_{h5}	5.588
L_{h1}	19.812	g	0.254
w_{h1}	23.114	p_1	11.43

Figure 3 illustrates that etching the fractal geometry onto the hexagonal radiating element and truncating the outer corners of the ground plane significantly a ffect t he upper frequency band: the operating bandwidth is broadened, and additional resonances are generated at higher frequencies, resulting in an 18.33% improvement in impedance bandwidth.

The real and imaginary components of the antenna's input impedance are plotted in Figure 4. The real part remains well matched across the entire operating bandwidth, staying close to the 50 Ω reference impedance of the excitation port. Moreover, the imaginary part oscillates consistently around zero

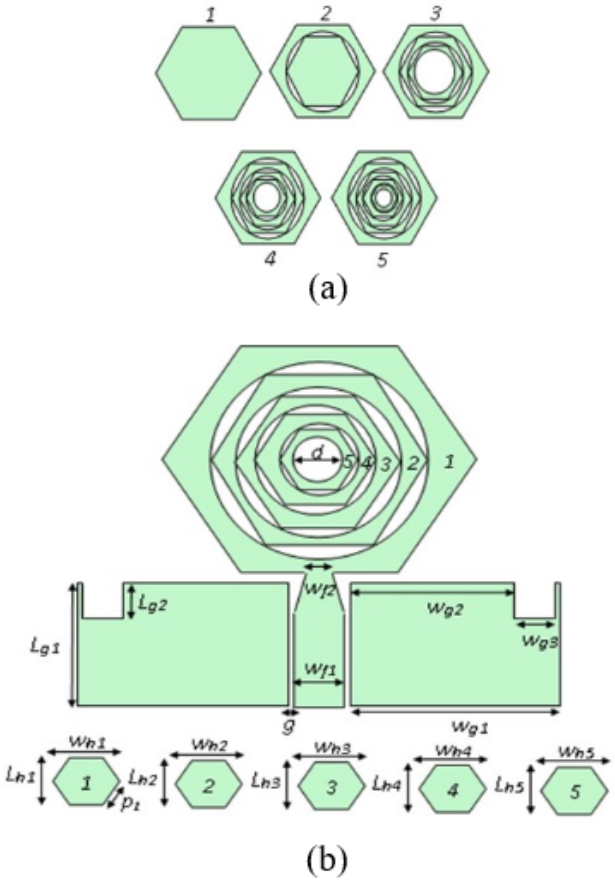

FIGURE 1. Configuration of the proposed UWB hexagonal fractal antenna, (a) Construction steps of the radiating patch, (b) Detailed configuration of the proposed UWB antenna.

over the operating band, confirming the broadband behavior of the proposed antenna and its suitability for the full UWB spectrum.

Surface current distribution analysis helps identify the contribution of different antenna regions to the overall bandwidth and resonant frequencies. Figure 5 shows the simulated current distributions at key resonances. At the first resonant frequency of 3.67 GHz (Figure 5a), the current is concentrated mainly in the central lower part of the antenna. This region therefore governs the low frequency impedance behavior. Additionally, the weak current observed along the fractal slots indicates that these etched structures contribute little to the excitation of the lower resonance.

Figure 3 confirms that the fractal modifications have minimal effect on the low frequency resonance (e.g., 3.67 GHz), as shown by the nearly identical reflection coefficients of the fractal and baseline antennas. At the mid band frequency of 7.2 GHz (Figure 5b), the current concentrates along the edges of the hexagonal patch and the center of the ground plane, largely avoiding the fractal etched regions. In contrast, at 10.41 GHz (Figure 5c), the current spreads uniformly across the radiator, indicating that the fractal slots promote multi-resonance coupling at higher frequencies. This frequency-

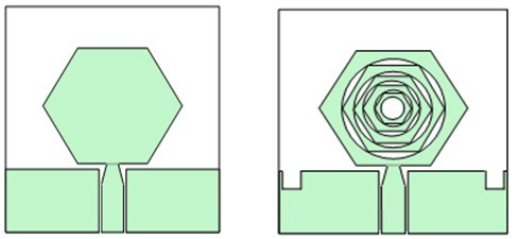

FIGURE 2. Antenna design evolution, (left) First antenna, (right) Final antenna

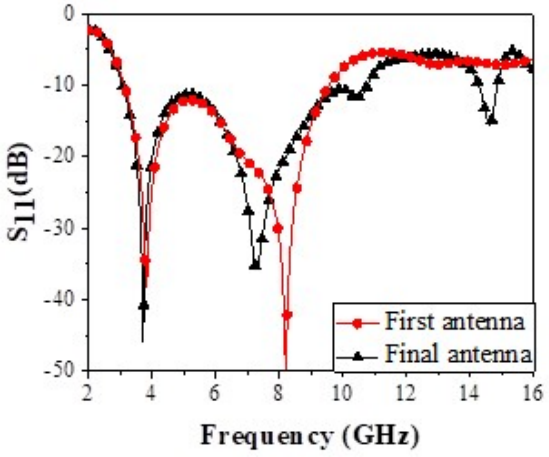

FIGURE 3. Role of the fractal geometry and of the amputated ground plane on the reflection coefficient of the antenna

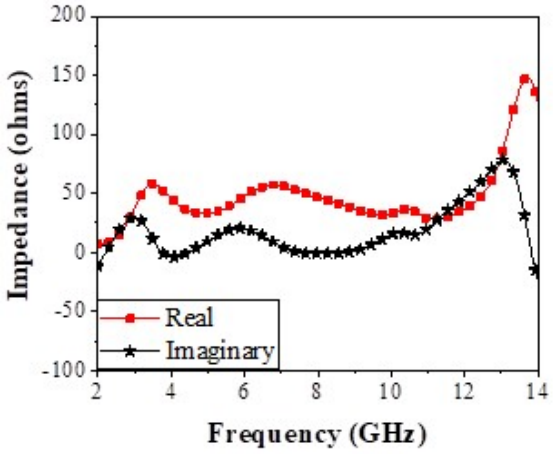

FIGURE 4. Real and imaginary impedance.

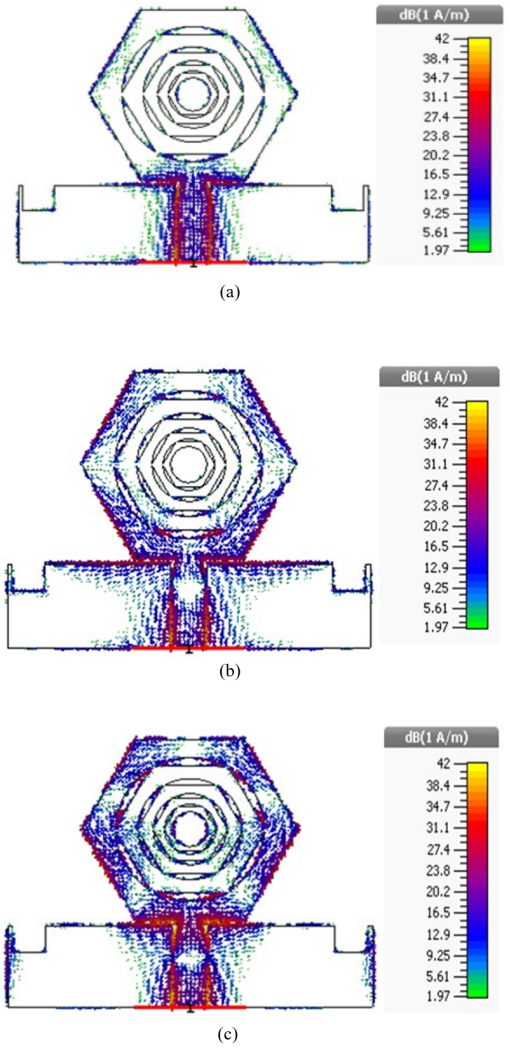

FIGURE 5. Current distribution on the antenna's surface at three frequencies (a) 3.67 GHz, (b) 7.2 GHz, and (c) 10.41 GHz.

dependent behavior demonstrates that the recursive slot pattern primarily enhances upper band performance, while the lower band response remains dominated by the unmodified radiator geometry.

The fabricated prototype (Figure 6), built on a 1.5 mm thick RO4350B substrate ($\varepsilon_r = 3.48$), measures $39.1 \times 36.6\,\text{mm}^2$, corresponding to $0.388\lambda_0 \times 0.364\lambda_0$ at 2.98 GHz. Measured S_{11} results obtained with an Agilent 8722ES VNA show close agreement with simulations (Figure 7), confirming an operating bandwidth from 2.98 to 11.8 GHz (119.35% fractional bandwidth), which exceeds the FCC UWB requirement by 9.35%. This bandwidth enhancement results from the fractal slots, which redistribute surface currents to excite additional resonances, together with the truncated ground plane edges that improve broadband impedance matching.

The measured co-polarized radiation patterns (Figure 8 and Figure 9), exhibit the expected omnidirectional behavior in the H-plane and bidirectional shape in the E-plane. Cross polarization remains below -12 dB in the H-plane over most of the band, rising slightly above 8 GHz due to diffraction from the slot edges and excitation of higher-order modes. Minor pattern distortion at frequencies above 9 GHz is consistent with ground plane edge reflections and the transition to a hybrid current distribution, as previously modeled in [18]–[20].

The antenna achieves a peak radiation efficiency of 95.78% at 10 GHz and maintains efficiency above 90% from 6 GHz onward (Figure 10), outperforming designs such as

that reported in [21]. Realized gain increases from 2.1 dBi at 3 GHz to 4.2 dBi at 10 GHz, overcoming the typical gain limitation of electrically small antennas at lower frequencies. As shown in Table 3, the proposed antenna demonstrates superior performance compared to the referenced designs across several key metrics. The antennas reported in [22]–[25] operate over multiple narrow frequency bands rather than a continuous ultra-wideband (UWB) range, and thus fail to cover the entire 3.1–10.6 GHz spectrum required for full UWB applications. In addition, their reported radiation efficiencies (75.6%, 95%, unreported, and 80%, respectively) are generally lower than that of the proposed antenna (95.8%). It is also noted that the efficiency of the design in [24] is not reported.

Similarly, the designs presented in [26]–[30] only partially cover the UWB band. Specifically, the antenna in [26] operates from 3.8 to 6.9 GHz (57.94% bandwidth), while [27] covers 2.93 to 9.53 GHz (105.94%), missing the upper portion of the UWB spectrum. The design in [28] exhibits a very narrow bandwidth (2.32–2.57 GHz), whereas [29] and [30] operate over 1.7–5.9 GHz and 2.2–5 GHz, respectively. None of these designs achieves continuous bandwidth coverage from below 3 GHz to above 10 GHz, as accomplished by the proposed antenna (2.98–11.8 GHz, corresponding to 119.35%).

Furthermore, the radiation efficiencies of [27]–[30] (90%, 95%, 89%, and 92%, respectively) remain lower than the 95.8% achieved by the proposed design. In terms of electrical size, certain antennas such as those in [26] and [28] exhibit larger dimensions compared to the proposed configuration ($0.388\lambda_0 \times 0.364\lambda_0 \times 0.015\lambda_0$), with sizes of $0.633\lambda_0 \times 0.633\lambda_0$ and $0.402\lambda_0 \times 0.549\lambda_0$, respectively.

Regarding maximum realized gain, the proposed antenna achieves 4.2 dBi, outperforming several designs such as [22] (2.5 dBi), [23] (3.98 dBi), [29] (3.5 dBi), and [30] (2 dBi). Although higher gains are reported in [24] (5.32 dBi) and [26] (6.32 dBi), these come at the cost of either unreported efficiency [24] or significantly larger electrical size [26].

In summary, the proposed antenna uniquely achieves a balanced combination of continuous ultra-wide bandwidth (2.98–11.8 GHz), high radiation efficiency (95.8%), competitive gain (4.2 dBi), and compact electrical dimensions. To the best of the authors' knowledge, none of the compared designs simultaneously satisfies all these performance criteria.

III. CONCLUSION

This study presents a compact, CPW-fed slotted hexagonal antenna optimized for UWB applications. By embedding a fractal geometry of five u niquely s haped s lots i nto the radiating patch and strategically truncating the ground plane, the design achieves a broad impedance bandwidth of 2.98–11.8 GHz (119.35%), exceeding the standard UWB spectrum. Measurements performed with an Agilent 8722ES vector network analyzer and in an anechoic chamber align closely with simulation results, validating the design. The antenna exhibits stable omnidirectional H-plane and bidirectional E-plane radiation patterns across the operating frequency range, with a peak radiation efficiency of 95.78%at 10 GHz and improved realized gain. The novelty of this work is fourfold: (i) a new hexagonal fractal geometry with five iterations of circular splits; (ii) an ultra wide band-width achieved with a compact electrical size ($0.388\ \lambda_0 \times 0.364\ \lambda_0 \times 0.015\ \lambda_0$); (iii) a systematic recursive scaling design method; and (iv) experimental validation showing excellent agreement with simulations. Collectively, these contributions demonstrate that the proposed design success-fully overcomes the typical trade offs between bandwidth, compactness, and radiation stability, positioning it as a strong candidate for modern UWB systems such as IoT, wearable devices, and high speed wireless communication.

FIGURE 6. Fabricated prototype of the proposed CPW-fed slotted hexagonal antenna.

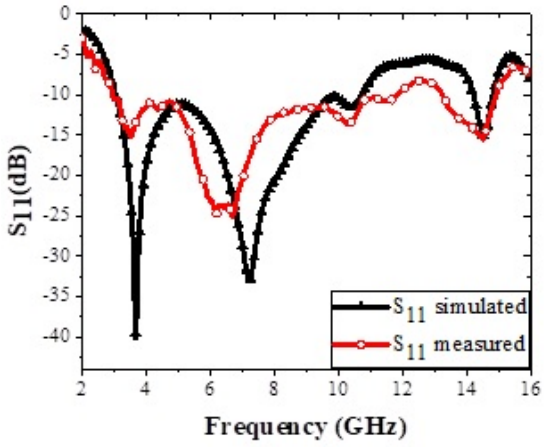

FIGURE 7. Measured and simulated reflection coefficients of the designed antenna.

ACKNOWLEDGMENT

This work is supported by the Ministry of Higher Education and Scientific R esearch o f A lgeria a s p art o f a research

TABLE 3. Comparison with Recent UWB Antennas

Reference	Size	Bandwidth ($S_{11} < -10$ dB)	Max Gain	Max Efficiency
[22]	$0.205\lambda_0 \times 0.301\lambda_0 \times 0.003\lambda_0$	3.61–5.28 GHz (38%) 2.35–2.6 GHz (8.06%)	2.5 dBi	75.6%
[23]	$0.18\lambda_0 \times 0.3\lambda_0 \times 0.12\lambda_0$	2.3–2.5 GHz (8.33%) 2.6–3 GHz (14.29%) 6.9–7.1 GHz (2.86%)	3.98 dBi	95%
[24]	$0.24\lambda_0 \times 0.192\lambda_0 \times 0.0128\lambda_0$	2.40–3.89 GHz (47.86%) 5.33–15.75 GHz (98.86%)	5.32 dBi	–
[25]	$0.109\lambda_0 \times 0.072\lambda_0 \times 0.0031\lambda_0$	0.584–1 GHz (52.53%) 3.24–4.32 GHz (28.57%)	4.55 dBi	80%
[26]	$0.633\lambda_0 \times 0.633\lambda_0 \times 0.02\lambda_0$	3.8–6.9 GHz (57.94%)	6.32 dBi	99%
[27]	$0.391\lambda_0 \times 0.234\lambda_0 \times 0.0156\lambda_0$	2.93–9.53 GHz (105.94%)	4.25 dBi	90%
[28]	$0.402\lambda_0 \times 0.549\lambda_0 \times 0.039\lambda_0$	2.32–2.57 GHz (10.23%)	4.3 dBi	95%
[29]	$0.255\lambda_0 \times 0.255\lambda_0 \times 0.0085\lambda_0$	1.7–5.9 GHz (110.53%)	3.5 dBi	89%
[30]	$0.293\lambda_0 \times 0.293\lambda_0 \times 0.0117\lambda_0$	2.2–5 GHz (77.78%)	2 dBi	92%
This work	$\mathbf{0.388\lambda_0 \times 0.364\lambda_0 \times 0.015\lambda_0}$	**2.98–11.8 GHz (119.35%)**	**4.2 dBi**	**95.8%**

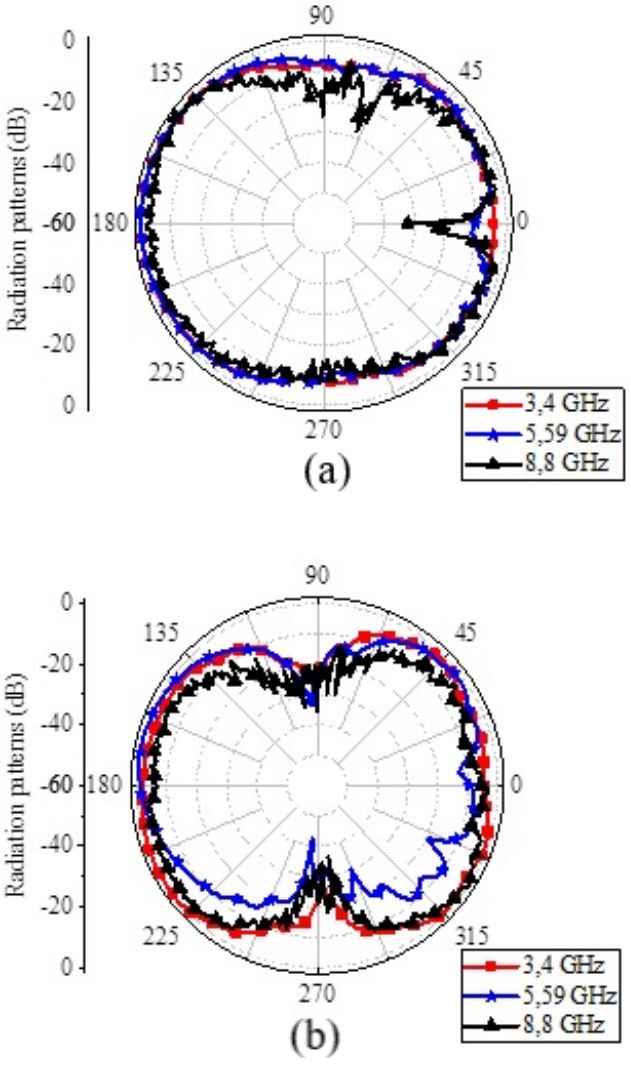

FIGURE 8. Measured normalized co-polarization radiation patterns at different frequencies, (a) xz-plane, (b) yz-plane.

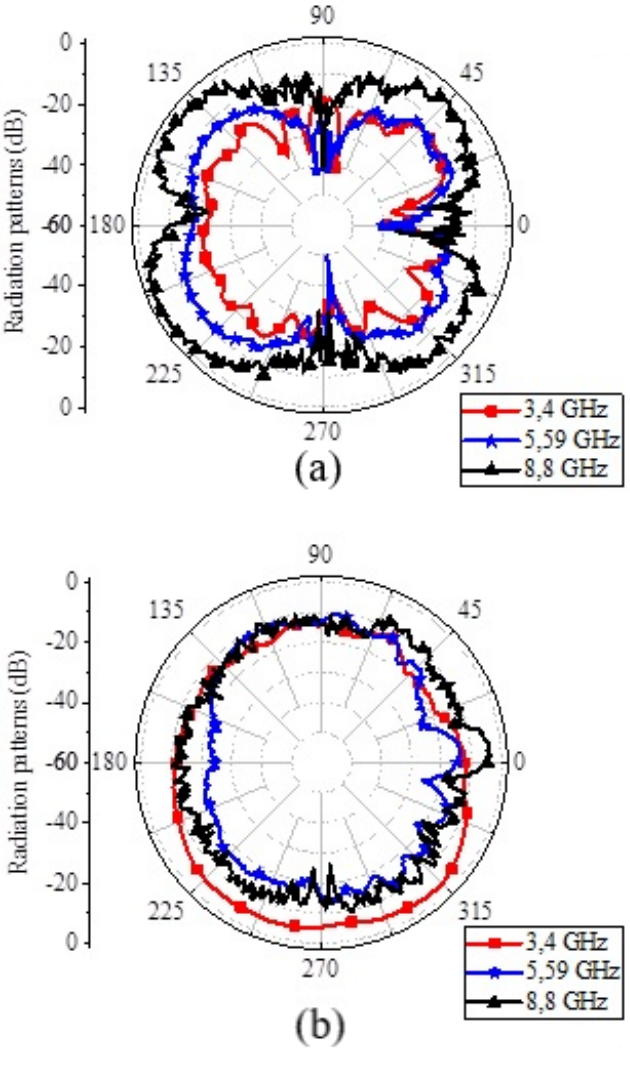

FIGURE 9. Measured normalized cross-polarization radiation patterns at different frequencies, (a) xz-plane, (b) yz-planee.

project (PRFU No. A25N01UN170120230003).

REFERENCES

[1] M. U. Ali, L. F. Abdulrazak, J. Iqbal, U. Illahi, G. I. Kiani, R. A. Khan, and H. Elmannai, "Design of an optimized low-profile UWB rectangular dielectric resonator antenna with moon-shaped ground for 5G–millimeter wave applications," Int. J. Electron. Commun., vol. 200, Art. no. 155903,

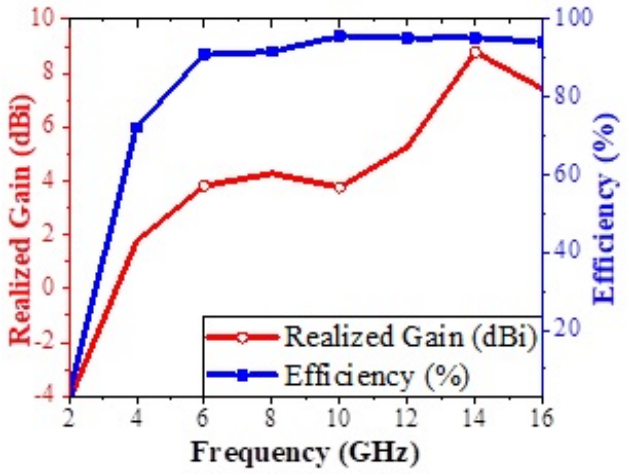

FIGURE 10. Realized gain and efficiency achieved by the designed antenna.

pp. 1–11, 2025.

[2] D. Aissaoui, A. Chaabane, A. Boualleg, and M. Guerroui, "Coplanar waveguide-fed UWB slotted antenna with notched-band performance," Period. Polytech. Electr. Eng. Comput. Sci., vol. 65, no. 1, pp. 69–73, 2021.

[3] R. Sahoo and D. Vakula, "A cylindrical wideband conformal fractal antenna for GPS application," Advanced Electromagnetics, vol. 6, no. 3, pp. 65–68, Oct. 2017.

[4] S. Alluri and N. Rangaswamy, "Compact high bandwidth dimension ratio steering-shaped super wideband antenna for future wireless communication applications," Microw. Opt. Technol. Lett., 2020.

[5] B. Guenad, A. Chaabane, D. Aissaoui, A. Bouacha, and T. A. Denidni, "Compact cauliflower-shaped antenna for ultra-wideband applications," Appl. Comput. Electromagn. Soc. J., vol. 37, no. 1, pp. 68–77, 2022.

[6] R. Sampath and K. T. Selvan, "Compact hybrid Sierpinski Koch fractal UWB MIMO antenna with pattern diversity," Int. J. RF Microw. Comput.-Aided Eng., vol. 30, no. 1, Art. no. e22017, 2020.

[7] X. Ran, Z. Yu, R. Niu, Y. Chang, and F. Wang, "A floral-like fractal ultra-wideband flexible antenna for wearable device," Int. J. RF Microw. Comput.-Aided Eng., Art. ID 8057773, 2025.

[8] A. Azzouz, R. Bouhmidi, M. E. Munir, M. M. Nasralla, and M. Chetioui, "Performance analysis of a high-gain multi-band wheel-shaped fractal antenna using Sierpinski carpet and Koch snowflake geometries," Results Eng., vol. 26, Art. no. 105328, pp. 1–9, 2025.

[9] S. Attioui, A. Khabba, S. Ibnyaich, A. Zeroual, Z. Zakaria, and A. J. A. Al-Gburi, "Design of a miniaturized circular flower-shaped fractal antenna with a defected ground structure for multiband applications," Prog. Electromagn. Res. C, vol. 155, pp. 203–211, 2025.

[10] S. A. Shandal, Y. S. Mezaal, and M. F. Mosleh, "Miniaturized wideband microstrip antenna for recent wireless applications," Adv. Electromagn., vol. 7, no. 5, pp. 7–13, 2018.

[11] R. H. Elabd, A. J. A. Al-Gburi, and A. A. Megahed, "Wideband 1×2 tree-shaped fractal antenna array with gain enhancement and sidelobe level reduction for sub-6 GHz 5G applications," Results Opt., vol. 21, Art. no. 100918, 2025.

[12] M. Shunmugathammal et al., "Flexible fractal loaded patch antenna for wearable application," Analog Integr. Circuits Signal Process., vol. 125, no. 2, pp. 2–17, 2025.

[13] Y. K. Choukiker and J. C. Mudiganti, "Compact hybrid fractal antenna for wideband wireless applications," Int. J. Microw. Wireless Technol., vol. 9, no. 5, pp. 1191–1196, 2017.

[14] S. Das, D. Mitra, and S. R. B. Chaudhuri, "Staircase fractal loaded microstrip patch antenna for super wide band operation," Prog. Electromagn. Res. C, vol. 95, pp. 183–194, 2019.

[15] K. V. Karad et al., "A SAR analysis of hexagonal-shaped UWB antenna for healthcare applications," EURASIP J. Wireless Commun. Netw., vol. 72, pp. 2–20, 2024.

[16] S. Attioui, A. Khabba, L. Aguni, S. Ibnyaich, and A. Zeroual, "Hybrid fractal antenna design for UWB applications inspired by Giuseppe Peano and Sierpinski carpet," Analog Integr. Circuits Signal Process., vol. 122, p. 29, 2025.

[17] M. Gupta and V. Mathur, "Hexagonal fractal antenna using Koch for wireless applications," Frequenz, vol. 72, no. 9–10, pp. 443–453, 2018.

[18] M. Guerroui, A. Chaabane, and A. Boualleg, "Super UWB grooved and corrugated antenna for GPR application," Period. Polytech. Electr. Eng. Comput. Sci., vol. 66, no. 1, pp. 31–37, 2022.

[19] A. Chaabane and M. Guerroui, "Printed UWB rhombus shaped antenna for GPR applications," Iran. J. Electr. Electron. Eng., vol. 17, no. 4, pp. 2041–2041, 2021.

[20] D. Aissaoui, A. Chaabane, and A. Bouacha, "Compact super UWB elliptical antenna with corrugations for wireless communication systems," in Proc. 1st Int. Conf. Innovative Res. Appl. Sci., Eng. Technol. (IRASET), 2020, pp. 1–4.

[21] T. Saeidi, I. Ismail, W. P. Wen, and A. R. Alhawari, "Ultra-wideband elliptical patch antenna for microwave imaging of wood," Int. J. Microw. Wireless Technol., vol. 11, no. 9, pp. 948–966, 2019.

[22] M. Shunmugathammal, C. Ajitha, F. D. Shadrach, N. Muthukumaran, K. A. Malar, A. Ahilan, P. Deepa, and P. Balamurali, "Flexible fractal loaded patch antenna for wearable application," Analog Integr. Circuits Signal Process., vol. 125, no. 2, pp. 1–17, 2025, doi: 10.1007/s10470-025-02475-0.

[23] S. Bhunia, K. Guha, and T. Tewary, "Hybrid shaped multiband microstrip patch antenna for wireless communication applications," J. Nano-Electron. Phys., vol. 16, no. 4, pp. 04017-1–04017-5, 2024.

[24] G. Bharti and J. S. Sivia, "Koch curves and hexagonal ring-shaped geometry based ultra-wideband fractal antenna," Wireless Pers. Commun., vol. 137, pp. 2535–2555, 2024, doi: 10.1007/s11277-024-11521-5.

[25] S. Rana, L. Kumar, A. K. Gautam, S. Sharma, and R. Rishi, "High gain, self-isolated S-shaped dual wideband MIMO antenna for 5G wireless applications," Wireless Pers. Commun., vol. 146, pp. 517–536, 2026, doi: 10.1007/s11277-025-11895-0.

[26] P. D. Kale, S. B. Patil, P. V. Deshmukh, D. P. Tulaskar, V. Bhope, D. Parkhi, Y. Thakare, and A. K. Shahade, "A novel quadband antenna with circular patch and modified Sierpinski gasket fractal ground structure for next-generation wireless communication system," J. Wireless Commun. Netw., vol. 2026, no. 35, pp. 1–27, 2026, doi: 10.1186/s13638-026-02588-8.

[27] V. Mathur, P. Tyagi, and V. K. Chandna, "Fractal ring shaped with saw feed microstrip patch antenna for wireless utilizations," Wireless Pers. Commun., vol. 138, pp. 2561–2582, 2024, doi: 10.1007/s11277-024-11614-1.

[28] R. Kalaiyarasan, G. Nagarajan, and R. S. Kumaran, "Design and implementation of an efficient Sierpinski carpet fractal antenna for 2.45 GHz applications," SN Comput. Sci., vol. 4, Art. no. 728, pp. 1–11, 2023, doi: 10.1007/s42979-023-02154-9.

[29] V. Subashini, S. Chitra, and S. Ramesh, "Performance analysis of multi-band frequency-reconfigurable antenna for cognitive radio applications," J. Wireless Commun. Netw., vol. 2026, no. 5, pp. 1–14, 2026, doi: 10.1186/s13638-025-02555-9.

[30] G. Kalkhambkar, R. Khanai, and P. Chindhi, "A novel snail shell inspired wideband fractal antenna for Internet of Things applications," Arab. J. Sci. Eng., vol. 48, pp. 15463–15474, 2023, doi: 10.1007/s13369-023-08079-y.